

## Object-based change detection in wind storm-damaged forest using high-resolution multispectral images

N. Chehata<sup>a,b\*</sup>, C. Omy<sup>a,c</sup>, S. Boukir<sup>a</sup>, D. Guyon<sup>c</sup>, and J.P. Wigneron<sup>c</sup>

<sup>a</sup>EA 4592 G&E, ENSEGID-IPB, University of Bordeaux, Pessac Cedex, France; <sup>b</sup>IRD, LISAH UMR 144, Tunis, Tunisia; <sup>c</sup>INRA, UMR 1391 ISPA, Villenave d'Ornon, France

(Received 2 April 2013; accepted 4 February 2014)

Natural disasters are generally brutal and may affect large areas, which then need to be rapidly mapped to assess the impacts of such events on ecosystems and to prevent related risks. Ground investigations may be complex, whereas remote-sensing techniques enable a fast regional-scale assessment of damage and offer a cost-effective option for large and inaccessible areas. Here, an efficient, quasi-automatic object-based method for change mapping using high-spatial-resolution (HR) (5–10 m) satellite imagery is proposed. Our contribution comprises two main novelties with respect to similar works in forestry. First, an automatic feature selection process optimizes the image segmentation and classification steps via an original calibration-like procedure. Second, an automatic bitemporal classification enables the separation of damaged and intact areas thanks to a new descriptor based on the level of fragmentation of the obtained regions. The mean shift algorithm is used in both the segmentation and classification processes. The method was assessed in a maritime pine forest using bitemporal HR Formosat-2 multispectral images acquired pre- and post-Windstorm Klaus, which occurred in January 2009 in southwestern France. The binary overall classification accuracy reached 87.8% and outperformed a pixel-based K-means classification with no feature selection. A thematic analysis of the results highlights the correlation between the ages of trees and their sensitivity to wind.

### 1. Introduction

In a climate change context, wind storms have become more and more frequent. Windfall damages have to be quickly mapped to prevent fire risks and to update the national forest inventory. Although ground investigations are complex due to the obstacles created by fallen trees, remote-sensing techniques enable rapid monitoring of large and inaccessible areas. This study aims to provide a binary map discriminating damaged and non-damaged areas using high-spatial-resolution (HR) (5–10 m) satellite imagery. Bitemporal 8 m multispectral Formosat-2 images, acquired pre- and post-Windstorm Klaus, which occurred on 24 January 2009 in southwestern France, were used for the map.

In the literature, previous studies in forestry have produced low-resolution maps (i.e. minimal mapping unit  $\approx 1$  ha), using medium- or high-spatial resolution sensors and focused essentially on defoliation (Franklin et al. 1995), clear-cut detection (Fraser, Abuelgasim, and Latifovic 2005; Desclée, Bogaert, and Defourny 2006; Huang et al. 2008; Liu et al. 2008; Conchedda, Durieux, and Mayaux 2008), or deforestation (Hayes and Cohen 2007; McRoberts and Walters 2012; Vibrans et al. 2013). Fewer studies have addressed more abrupt and smaller-scale structural changes, such as windfall damage (Meyer, Geldreich, and Yesou

---

\*Corresponding author. Email: [nesrine.chehata@ensegid.fr](mailto:nesrine.chehata@ensegid.fr)

2001; Liu et al. 2008; Kennedy et al. 2009; Wang and Xu 2010; Jonikavičius and Mozgeris 2013). Moreover, the above works have generally utilized pixel-based approaches based on medium-spatial resolution sensors, such as Landsat TM or MODIS.

Bitemporal change detection methods can be based on either post-classification approaches that compare two classifications obtained separately using remotely sensed data from two dates (McRoberts and Walters 2012; Liu et al. 2008), or the direct classification of two sets of remotely sensed data that have been merged into a single dataset (Hayes and Cohen 2007). Post-classification approaches are robust to radiometric differences between images and provide accurate ‘from-to’ change information (Im and Jensen 2005) but suffer from segmentation and classification error propagation. Most post-classification approaches are pixel-based. Joint-classification approaches provide more information with which to classify small changes. They can rely on machine-learning algorithms using a training set (Im and Jensen 2005), expert knowledge (Fraser, Abuelgasim, and Latifovic 2005), or, alternatively, thresholding, which involves a parametric statistical test (Desclée, Bogaert, and Defourny 2006). In this work, the proposed method is based on bitemporal joint classification of forest damage (damaged vs. non-damaged).

Storm damage assessment using multispectral images can be separated into two approaches: (1) storm damage modelling based on image descriptors and (2) storm damage mapping using image classification methods. In the first approach, the relationships between image descriptors and forest variables are assessed – for example, the relationship between NDVI variation and the proportion of damaged area per pixel (Wang et al. 2010) or between image texture and the percentage of crown loss (King et al. 2005). However, the correlations obtained are insufficient for accurate damage mapping (Olthof, King, and Lautenschlager 2004; King et al. 2005). The second approach includes time-consuming traditional visual interpretation of imagery (Clandillon, Yesou, and Meyer 2003) and few automated methods. Some authors (Olthof, King, and Lautenschlager 2004; Meyer, Geldreich, and Yesou 2001) have proceeded with a traditional pixel-based supervised classification using differencing images and vegetation indices, whereas Schwarz, Steinmeier, and Waser (2001) used a supervised object-oriented classification considering four spectral bands. The proposed method is based on a binary joint classification of forest storm damage.

Given the increasing spatial resolution of new satellites, various methods have been developed to exploit contextual spatial information. Some approaches use regional per-pixel descriptors before a pixel-wise classification (King et al. 2005; Fraser, Abuelgasim, and Latifovic 2005; Im and Jensen 2005; Franklin et al. 1995). Recently, the use of object-based image analysis (OBIA) has increased in the remote-sensing community (Benz et al. 2004; Blaschke 2010). In forestry, object-based classifications are used for structure mapping (Mallinis et al. 2008; Lamonaca, Corona, and Barbati 2008; Johansen et al. 2007; Mäkelä and Pekkarinen 2001; Pasher and King 2009) and for change detection (Desclée, Bogaert, and Defourny 2006; Schwarz, Steinmeier, and Waser 2001; Conchedda, Durieux, and Mayaux 2008; Wulder et al. 2008; Chehata et al. 2011). The OBIA approach is based on a segmentation process that combines spatial and spectral information to group pixels into homogeneous regions before their classification using new object descriptors. These object descriptors can be geometrical and textural (Fraser, Abuelgasim, and Latifovic 2005) or temporal (Desclée, Bogaert, and Defourny 2006; Chehata et al. 2011). Bitemporal object-based analysis has the advantage of reducing misregistration and shadowing effects compared with a pixel-based approach (Johansen et al. 2010).

Various segmentation algorithms are used in the forestry literature, the most common being a region-growing algorithm that minimizes intra-region variance (Kim, Madden, and Warner 2008; Desclée, Bogaert, and Defourny 2006) generally using Definiens

Imaging 2004 software (Benz et al. 2004). Mäkelä and Pekkarinen (2001) used the Narendra and Goldberg segmentation algorithm to group pixels according to a heterogeneity measure based on local gradients. Liu et al. (2008) used a supervised Markov random field for segmentation and classification with good results for detection of areas of severe and large forest change. The mean shift (MS) algorithm has also exhibited satisfactory results for remote-sensing image segmentation applications such as individual tree crown delineation from aerial images (Wang, Soh, and Shultz 2006) or agricultural land delineation (Ozdarici and Akyurek 2012). To our knowledge, the MS algorithm has not been used for forest cover mapping. It will be detailed in Section 3.2.

The proposed method is an object-based, bitemporal classification that maps storm damage at a fine spatial scale. It is nearly automatic, requiring limited training data to rapidly map damage over a wide area.

## 2. Study area and data

The Nezer forest covers approximately 60 km<sup>2</sup> and is located near the Atlantic coast in southwest France, within a large European maritime pine (*Pinus pinaster* Ait.) forest. The forest is made up of rectangular stands of pine trees of similar age and height. Stand age varies from seedling to 55 years, density from 150 to 3000 trees ha<sup>-1</sup>, and tree height from 0 to 25 m, as reported in Garestier et al. (2009). The maximum crown diameter reaches approximately 8 m for the oldest stands (Guyon et al. 2005).

Bitemporal Formosat-2 images from pre- and post-Windstorm Klaus, acquired on 22 December 2008 and 4 February 2009, respectively, were used (Figure 1). The images

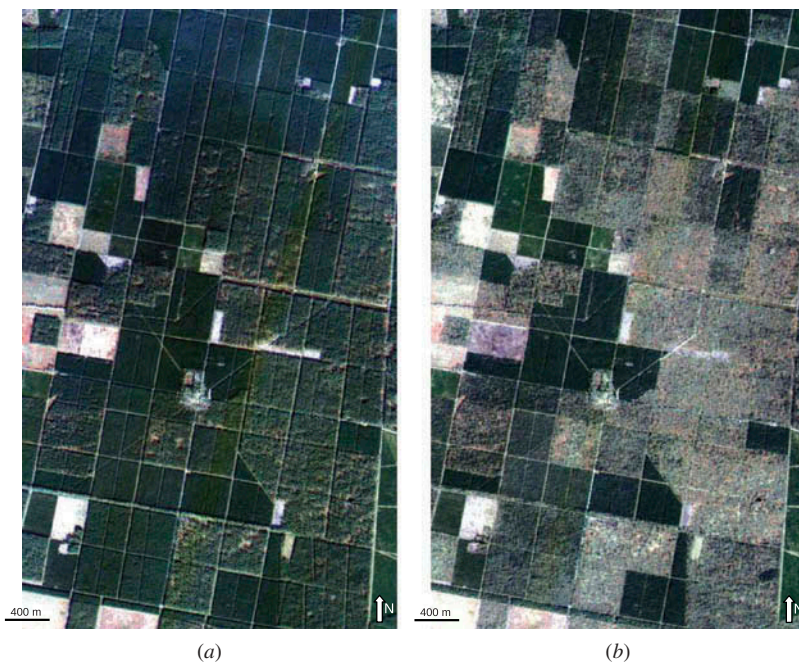


Figure 1. Formosat-2 multispectral images acquired before and after Windstorm Klaus.

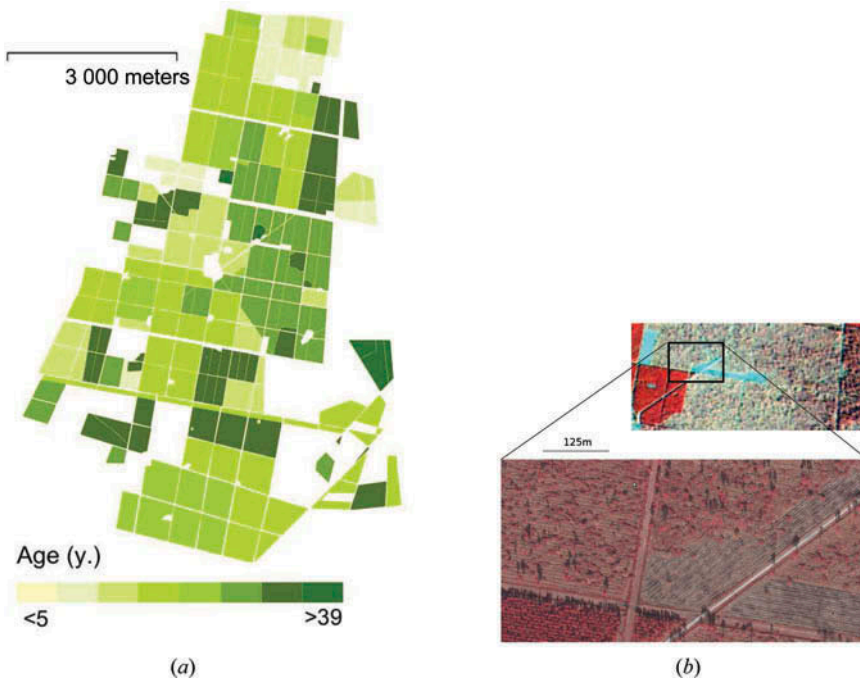


Figure 2. Ancillary data: (a) geodatabase of stand ages and (b) 15 cm-resolution colour infrared aerial photograph acquired after the storm (26 February 2009).

have 8 m spatial resolution and four spectral bands (blue (B), green (G), red (R), and near-infrared (NIR)). Image radiance was converted into TOA (top-of-atmosphere) reflectance and rescaled between 0 and 255. Both images were orthorectified and georeferenced. Ancillary data include a GIS layer of tree stand delimitations and ages provided by the INRA<sup>1</sup> geodatabase for the Nezer site (Figure 2(a)).

In addition, 100 reference areas (damaged vs. non-damaged) were identified on 15 cm-resolution colour infrared photographs acquired after the storm (Figure 2(b)). The visual interpretation of these images was complex due to the variety of damage types (bent, fallen, uprooted, and broken-topped trees). Consequently, to minimize damage identification errors, reference areas were identified and delineated as either non-damaged or completely damaged. The size of the reference areas varied between 198 m<sup>2</sup> (around 3 pixels) and 23,128 m<sup>2</sup> (around 260 pixels), with an average of 4806 m<sup>2</sup> (around 75 pixels). All age classes were sampled in both categories (damaged and non-damaged) except for stands younger than five years, in which the damage was limited to bent trees and was difficult to distinguish visually.

The youngest damaged samples (5–13 years) were essentially bent trees. The 14–19-year-old damaged samples were represented by bent, fallen, or uprooted trees. For trees older than 20 years, all damage types were observed (i.e. bent, fallen, uprooted, and broken-topped trees). The oldest damaged samples (>25 years) were primarily groups of uprooted trees. Intact reference areas were also delineated for all age classes. However, intact areas were in the minority for the oldest classes, which were severely damaged by the storm.

### 3. Methodology

The proposed method is an object-based, bitemporal classification of storm damage. In the following section, selected image features are presented. MS segmentation, which is at the core of our algorithm, will be detailed. Then, the automatic feature selection process will be explained and finally the automatic object-based bitemporal classification method will be presented.

#### 3.1. Proposed input features

Input features can be grouped into three main categories: spectral, textural, and temporal (Table 1). For spectral features, the Formosat-2 spectral bands (B, G, R, NIR) were used as well as two vegetation indices, the normalized difference and soil adjusted vegetation indices (NDVI and SAVI, respectively). First-order statistics, such as the mean and variance of the reflectance, were used as textural features. Among the more commonly used texture features are the Haralick features (derived from a grey level co-occurrence matrix) (Haralick, Shanmugam, and Dinstein 1973), and some of these are considered particularly relevant for forest applications of image analysis (Ruiz, Fdez-sarria, and Recio 2004; Kayitakire, Hamel, and Defourny 2006; St-Louis et al. 2006; Trias-Sanz, Stamon, and Louchet 2008; Tuominen and Pekkarinen 2005). The neighbourhood radius and displacement vector length were both experimentally set to 1 pixel, which corresponds to a maximum crown diameter of 8 m. The displacement vector orientation was horizontal. Finally, three common temporal features were considered: mean correlation, difference, and ratio between the pair of images. Temporal and textural features were processed for each spectral band. A total of 84 features were used: 6 spectral features in addition to 10 textural and 3 temporal, all of the latter computed separately for each of the 6 spectral features.

#### 3.2. MS segmentation

The MS algorithm is a non-parametric, feature-space analysis technique that has shown excellent results in colour image clustering and object delineation (Fukunaga and Hostetler 1975; Comaniciu and Meer 2002). It is based on a density mode searching and clustering technique. The feature space is considered the empirical probability density function (PDF) of the input features. The algorithm proposes a filtering step that associates each pixel in the image with the closest local mode in the density distribution of the feature space. The MS procedure locates these modes without estimating the global density. Then, the fusion of the regions associated with nearby modes leads to image segmentation. The implementation of the method proposed by Comaniciu and Meer (2002) searches for local modes in the joint feature and spatial domain of  $n + 2$  dimensions, where  $n$  is the number of features added to

Table 1. Spectral, textural, and temporal input features.

Spectral	Textural	Temporal
Blue	Mean	Difference
Green	Variance	Ratio
Red	8 Haralick features	Mean correlation
NIR	Mean, contrast, entropy	
NDVI	Angular second Moment	
SAVI	Inverse difference moment, sum average, sum entropy, sum variance	

the two dimensions of the spatial domain. An iterative procedure of mode seeking consists of shifting the  $n + 2$  dimensional window to a local mode.

The search window involves two user-defined inputs that can be deduced from the desired object sizes or physical properties. A radiometric range ( $h_r$ ) corresponds to the unique spectral radius in the  $n$ -dimensional search window and a spatial bandwidth ( $h_s$ ) that corresponds to the spatial radius of the window. To extract the objects of interest (i.e. tree stands),  $h_r$  should be (1) higher than the maximum radiometric difference between intra-region pixel pairs and (2) lower than the radiometric difference between region pixels and surrounding pixels outside the region. In practice,  $h_r$  is optimized by the automatic feature selection process (see Section 3.3). All features were individually rescaled between 0 and 255, and radiometric range  $h_r$  varied from 2 to 60. The value of  $h_s$  should be close to the size of the objects of interest. In fact, the  $n + 2$ -dimensional moving window for mode searching should remain spatially within the object of interest such that all of its pixels are associated with a local mode within the window. Figure 3 illustrates the impact of both parameters on the segmentation results.

The spatial radius  $h_s$  of the MS segmentation was set using prior thematic knowledge of the desired object size. Using  $h_s = 3$ , the spatial window can reasonably be considered a regular forest pattern (Orny et al. 2010). Finally, in the proposed method, the MS procedure is used in both segmentation and classification steps using the joint spatio-spectral domain and solely the spectral domain, respectively (see Section 3.4).

### 3.3. Automatic feature selection for segmentation

In the literature, segmentation is usually processed on all available before- and after-image bands (B, G, R, NIR) (Mäkelä and Pekkarinen 2001; Mallinis et al. 2008) or on derived

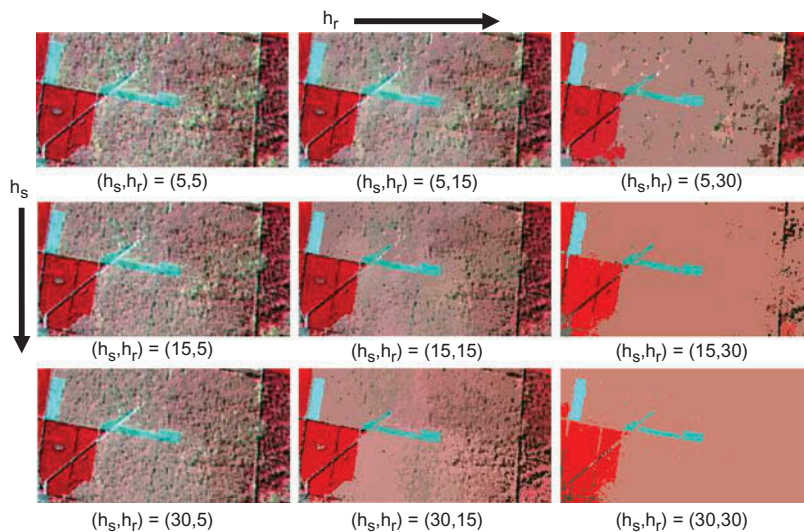


Figure 3. Mean shift segmentations of a four-channel image (B, G, R, NIR) using different parameters ( $h_s, h_r$ ). When  $h_r$  increases, only highly contrasted and homogeneous regions remain (e.g. the intact young stand on the left, the blue farming area, and the medium-aged stand on the right). If  $h_s$  increases, only larger regions remain: shadow areas and standing tree groups disappear within the central, strongly damaged area.

bands such as NDVI, SAVI, or transformed bands (PCA) with no feature selection (Wang and Xu 2010). Supervised feature selection for classification can be based on the modeling results of physical variables. In King et al. (2005), the image texture features best correlated to the percentage of crown loss were used for damage classification. In Trias-Sanz, Stamon, and Louchet (2008), a quantitative measure between segmented region boundaries and a reference GIS layer enabled the selection of the best features from among radiometric and texture features.

3.3.1. Feature selection using test frames

In this study, to determine the most relevant features for segmentation, input feature selection was carried out through an original generic calibration-like procedure using a test frame. Generally, a test frame is an ensemble of reference images that are used to calibrate cameras. In this study, this process was used to select the best features for segmentation and also aimed at automatically optimizing the segmentation parameters.

Classes describing different forest development stages and structures were defined. The number of classes was denoted as  $N_c$ . For the Nezer site, the age GIS reference layer and photointerpretation were used. The test frames were then constructed with  $N_c$  small non-overlapping image samples corresponding to  $N_c$  classes, yielding as many test frames as input features. The test frames were then segmented by the MS algorithm using one input feature (single test frame) and multiple rescaled features (multiband test frame) while simultaneously testing various segmentation parameterizations. All features were individually rescaled between 0 and 255. The feature segmentation performance (SP) is defined as

$$SP = \frac{1}{nc} \sum_i \max_j \left[ \frac{A(R_i \cap R_{s_j})}{A(R_i)}, R_i \cap R_{s_j} \neq 0 \right], \tag{1}$$

where  $A$  is the area,  $N_c$  the number of test frame classes,  $R_i$  is a test frame region, and  $R_{s_j}$  a segmented region that intersects  $R_i$ .  $i$  and  $j$  are the test frame and segmented region indices, respectively. SP depends on the regions' overlap percentage. Figure 4 illustrates an example of a test frame for after-storm segmentation with four samples and the corresponding SP computation. The highest SP value indicates the best feature or set of

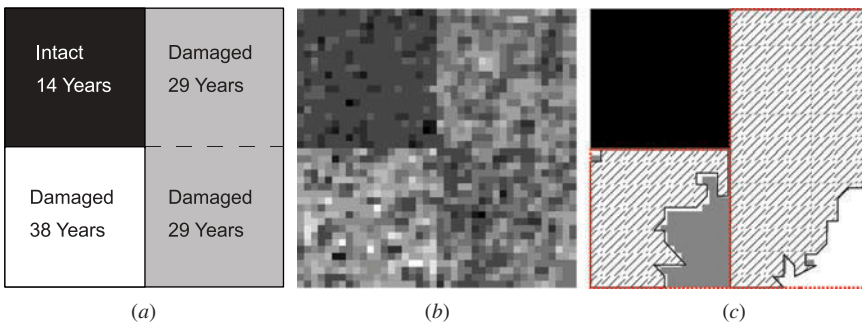


Figure 4. (a) Actual regions, (b) NIR band test frame, and (c) segmented regions using  $(h_s, h_r) = (5, 10)$ . Maximum overlaps per region are hatched. Segmentation performance (SP) = 86%.

features. In this study, test frames were constructed for each feature with four reference regions of  $20 \times 20$  pixels (Figure 6).

Automatic feature selection is applied in three steps: (1) segmentation into structurally homogeneous before-storm regions, (2) segmentation of the after-storm image into temporally and structurally homogeneous regions, and (3) binary change classification. As shown in Figure 6, reference test frames were adapted to each step using (1) actual age classes, (2) classes combining actual age and change type, and (3) actual change classes, respectively. For step (1), temporal features were not used, and for binary classification (step 3), only temporal features averaged over-segmented after-storm regions were used.

SP and the optimal  $h_r$  were then processed automatically based on the reference test frames to select the best features for each step.

### 3.4. Unsupervised object-based bitemporal classification

The global unsupervised object-based bitemporal change detection scheme is depicted in Figure 5. We assume that the degree of change depends not only on the type and intensity of the damage but also on the initial stand structure. Consequently, the before- and after-storm images are segmented independently using the MS algorithm. The before-storm segments correspond to homogeneous structural regions (i.e. those belonging to the same age class). The after-storm segments reflect the degree of change. The selected features are processed as explained in Section 3.3. The joint classification is based on the MS algorithm and is detailed in the current section.

#### 3.4.1. MS spectral classification

The after-storm segmented regions are characterized by object mean temporal descriptors (i.e. by temporal features that are averaged per region). The automatic feature selection process (see Section 3.3) provides the input features that optimize the MS spectral classifier. They are then clustered automatically into change classes using this optimized MS spectral classifier. Unlike MS segmentation (Comaniciu and Meer 2002), this modified version is independent of pixel positions and involves only the spectral domain, which allows the clustering of similarly damaged regions that are spatially distant into the same change class. The MS classifier has a single parameter,  $h_r$ , which is the radiometric range of the MS mode-seeking window. The lower the value of  $h_r$ , the lower a cluster's intra-variance.

MS spectral classification leads automatically to many change clusters. We did not seek to interpret the significance of these change classes, which would have required collecting specific reference data just after the storm. Our objective in the present study was to produce a damage map with a minimum of field data and an unsupervised classification process. Consequently, in this study, our work was limited to the production of a binary change map even when the MS spectral classification provided multiple change classes. A minimal radiometric range of  $h_r = 2$  was used to detect subtle changes (Figure 6). In this context of fine change detection, the number of change clusters can be high, and the spectral distinction between intact and lightly damaged regions may be complex. Thus, the automatic grouping of change clusters into damaged vs. non-damaged classes is challenging. To address this issue, an innovative spatio-temporal feature, the fragmentation rate, is proposed.

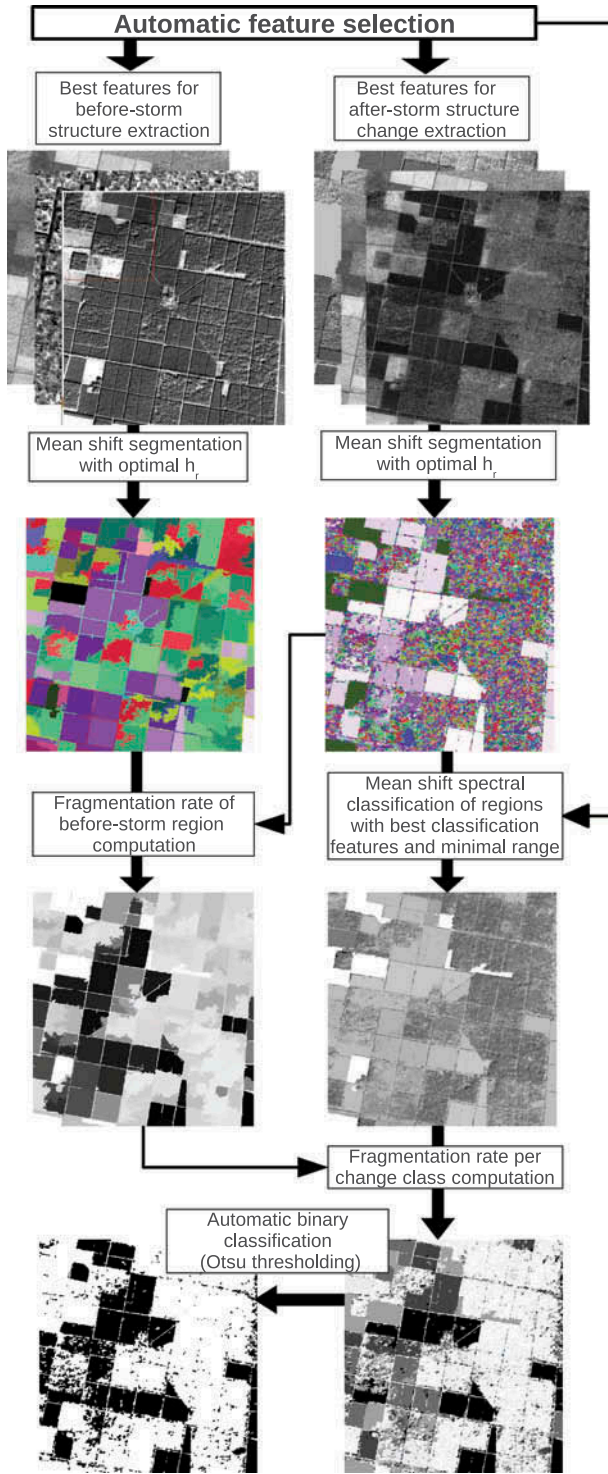


Figure 5. Bitemporal object-based change detection scheme illustrated over a  $3 \times 3, 3 \text{ km}^2$  area.

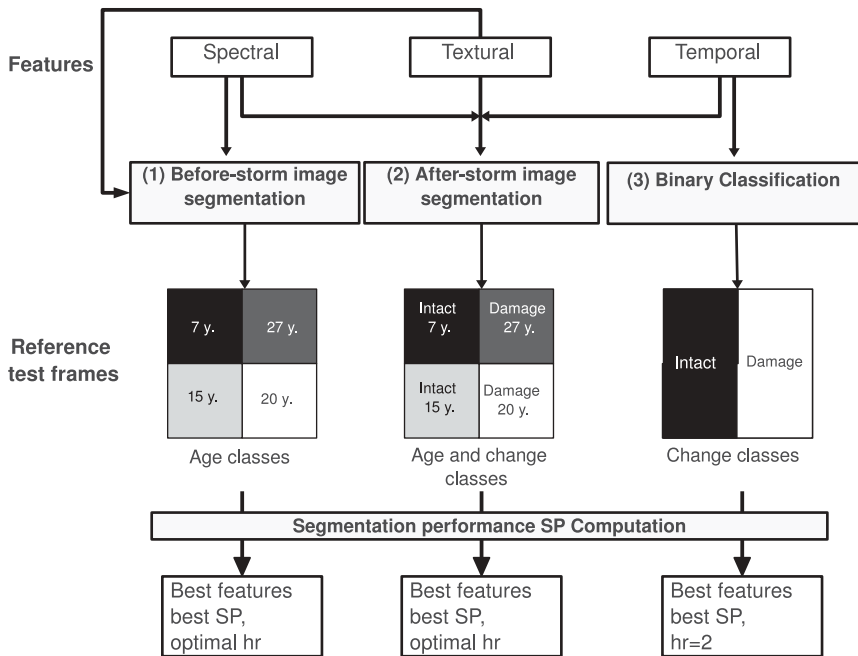


Figure 6. Automatic feature selection process.

3.4.2. A new spatio-temporal descriptor

To automatically group the change clusters into damaged vs. non-damaged classes in a robust way, the clusters were characterized by a new spatio-temporal feature: the fragmentation rate (FR). This idea is based on the fact that, generally, for a change detection application, landscape complexity increases with time. The diversification and fragmentation of a landscape lead to more heterogeneous regions in the image. The presence of heterogeneity (more or less important) in an initially homogeneous area can be interpreted as a change. Fragmentation would be more important in the case of disastrous changes such as storms, floods, or earthquakes than for progressive changes such as urbanization. In this study, damaged areas are heterogeneous and therefore appear over-segmented in the after-storm image. Conversely, intact areas correspond to larger regions that have similar delimitations in both images. FR characterizes the before-storm regions and reflects their over-segmentation in the after-storm image. It is computed as a comparison between the before- and corresponding after-storm regions, as follows:

$$FR(R_t) = 1 - \frac{\max_j [A(R_t) \cap A(R_{t+dt}^j)]}{A(R_t)}, R_t \cap R_{t+dt}^j \neq 0, \tag{2}$$

where  $A$  is the region of interest,  $R_t$  is the before-storm region, and  $R_{t+dt}^j$  the after-storm regions that are included (partly or entirely) in the before-storm one where  $j$  is the after-storm segmented regions index. The more the region  $R$  is fragmented, the nearer FR is to 1. Conversely, intact regions should have a low FR close to 0.

The average FR is then computed for the after-storm change clusters. The change cluster FR is then defined as

$$FR(CC) = \frac{1}{N} \sum_{p \in CC} |[FR(R_t(p))]|, \quad (3)$$

where CC is the after-storm change cluster and  $N$  the number of corresponding pixels ( $p$  represents a pixel). The FR per change cluster is the averaged FR of corresponding before-storm regions. The change clusters are finally divided into damaged vs. non-damaged classes, based on their FR and using the unsupervised Otsu threshold (Otsu 1979) which minimizes intra-class variance.

## 4. Results and discussion

### 4.1. Feature selection

The segmentation and classification steps for the selected features using mono- and multiband test frames are presented in this section.

#### 4.1.1. Feature selection for segmentation

Table 2 presents the segmentation performance SP (Equation (1)) and MS parametrization for segmentation steps (1) and (2) presented in Section 3.3.1.

One may observe that the best features for segmenting before- and after-storm images are related to the red bands. In fact, as shown by Guyon, Courier, and Berbigier (2001) for the same Nezer forest site, the pine crown cover fraction, related to tree density and crown size, explains a large part of the variability of red reflectance whereas NIR reflectance depends more strongly on the green biomass of pine trees and undergrowth vegetation. These properties of the red band are important in describing the forest structure before the storm (i.e. the forest variables determining the cover fraction of standing trees) and in detecting their changes after the storm (i.e. the broken, uprooted, or fallen trees that reduce the crown cover fraction without an immediate change in green biomass).

The best feature for the after-storm segmentation is temporal. The information on the initial stand structure (which depends on tree age) from before the storm helps to determine the degree of change after the storm.

Table 2. Optimal features and radiometric ranges,  $h_r$ , for after- and before-storm segmentations using a four-region test frame. SP is segmentation performance.

After-storm segmentation			Before-storm segmentation		
Feature	$h_r$	SP (%)	Feature	$h_r$	SP (%)
Red ratio	17	87.2	Red	2	80.7
Red	3	78.1	NDVI	3	77.3
Green ratio	16	75.5	Green	5	68.7

From Table 2, one may also observe that the maximal SP value is higher when segmenting the after-storm image (87.2%) than the before-storm (80.7%). In fact, the after-storm regions are better discriminated because they combine age class and type of change information, whereas before-storm regions differ only by age classes, which are not easily discriminated.

The optimal features for both segmentations are essentially spectral or temporal but not textural. This is most likely due to, on one hand, the spatial resolution of Formosat-2 (8 m), which provides insufficient textural information in a forest context, and on the other hand, the Haralick parameters not being optimized.

One may observe that the best SP values were obtained using only one feature. Multi-feature segmentation appears to be less relevant in this study, which can be explained by two factors. First, the chosen implementation of MS (Comanicu and Meer 2002) involves one unique radiometric range,  $h_r$  for multiple features. An adaptive MS radiometric range for each feature would enhance the results, as that approach would be more appropriate for remote-sensing images where the reflectance distribution varies for each spectral band. Second, forest canopies are very complex, and changes in their reflectance between the before- and after-storm images are correlated to other changes beyond structural changes following storm damage. For instance, some changes may be detected due to forest phenology or differences in shadows. Using only one feature may limit these detections, considered as misclassifications for the damage class.

#### 4.1.2. Feature selection for classification

The feature selection for the binary classification into damaged vs. non-damaged classes is shown in Table 3. Mono- and multiband two-region test frames were used (see Section 3.3.1). Only temporal features were tested (see Section 3.1). The best-performing feature was the green band difference, with a high SP value of over 92.6%. This was therefore used as an input for the MS classifier to establish the change classes (see Section 4.4). As with feature selection for segmentation, multiple features did not provide better results.

#### 4.2. MS segmentation

Figure 7 depicts the segmentation results before and after the storm using the corresponding best features. One can visually distinguish the intact and damaged areas. Intact areas are larger and have similar delimitations in both segmentations, whereas the damaged areas are more heterogeneous, leading to over-segmented regions.

Table 3. Optimal features for binary classification using a two-region test frame with  $h_r = 2$ .

Feature	SP (%)
Green difference	92.6
NIR difference	70.5
Red difference	64.5

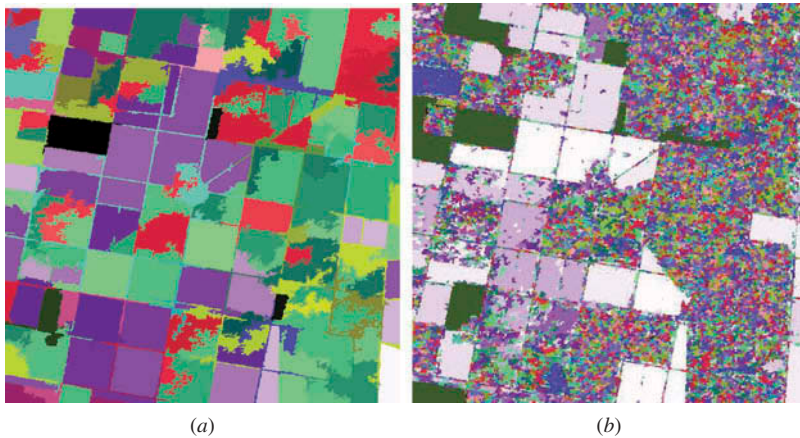


Figure 7. Segmentation of before- and after-storm images using the best features (i.e. red band and red band ratio, respectively).

#### 4.3. FR

Figure 8 illustrates the FR of before-storm segments in grey levels. The lighter the regions, the more damaged they are. This result visually matches the tree stand age map, where older stands appear to have more extensive damage than younger stands. In fact, among numerous factors, tree height most strongly influences the sensitivity of a tree to the wind (Cucchi et al. 2005). The young stands are dense with small trees, which makes them more robust to the wind. In contrast, older stands are less dense and more heterogeneous due to silvicultural practices and are composed of taller trees that are more vulnerable and likely to be damaged by storms.

#### 4.4. MS binary classification

The MS classifier is based exclusively on the spectral domain. After-storm segmented regions are classified into change clusters. Figure 9(a) shows approximately 30 change clusters

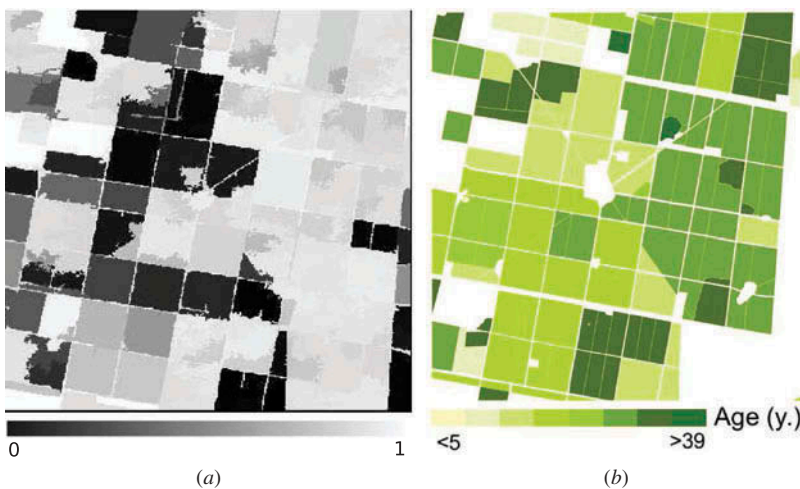


Figure 8. Comparison between fragmentation rate and tree stand ages.

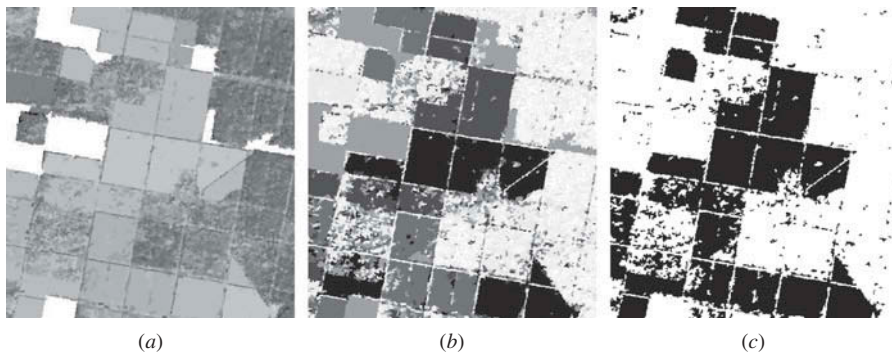


Figure 9. MS spectral classification and fragmentation rate for automatic binary mapping of forest storm damage.

created using the MS spectral classifier. Given the histogram complexity of this image, it is hard to automatically separate the obtained clusters into damaged vs. non-damaged classes. By contrast, one may observe (Figure 9(b)) that after characterization of these regions by their average FR (3)), the damaged areas are better discriminated. Figure 9(c) shows the result of an automatic binary classification achieved using Otsu thresholding.

#### 4.5. Map validation

##### 4.5.1. Comparison to a pixel-based approach

Our classification method was compared to an unsupervised pixel-based approach based on the well-known  $k$ -means clustering algorithm (Duda, Hart, and Stork 2001) and using all available image bands before and after the storm (eight bands) (i.e. without any feature selection process). The temporal feature used was the band difference, as our feature selection process indicated its efficiency for binary classification (see Section 4.1.2).

Table 4 shows the global confusion matrices obtained by comparing the pixel values from the classification results to reference data for both methods. The object-based

Table 4. Confusion matrices for binary classification (damage vs. non-damage) using our object-based approach with feature selection and a K-means pixel-based approach without feature selection.

	Ground truth		Total	Commission error (%)
	Undamaged	Damaged		
<b>Object-based approach</b>				
Undamaged	1436	459	1895	24.22
Damaged	81	2452	2533	3.2
Total	1517	2911	4428	
Omission error (%)	5.34	15.77		
Overall accuracy (%)	87.80			
<b>Pixel-based approach</b>				
Undamaged	1361	788	2149	36.67
Damaged	156	2123	2279	6.85
Total	1517	2911	4428	
Omission error (%)	10.28	27.07		
Overall accuracy (%)	78.68			

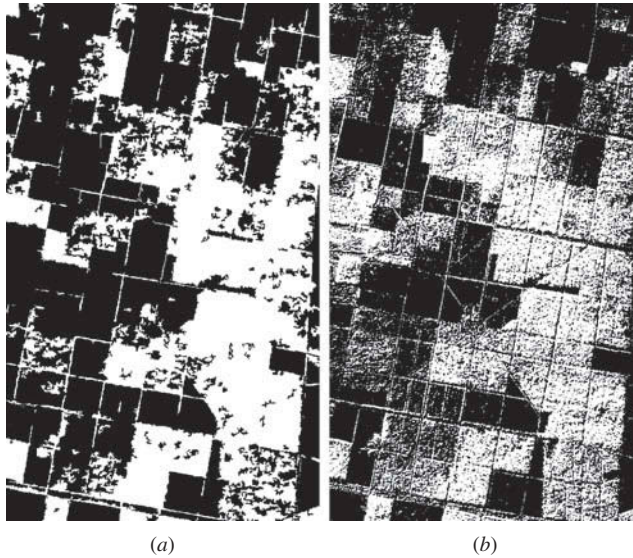


Figure 10. Change detection maps. Damaged vs. non-damaged areas are depicted in white and black, respectively.

approach outperformed the pixel-based approach with an overall classification accuracy of 87.8% vs. 78.7%, respectively. This result confirms the relevance of automatic feature selection and the new fragmentation descriptor to the proposed change detection scheme.

Additionally, one may observe that omission and commission errors were twofold less important for our method than for the pixel-based method. Few omission errors were obtained in non-damaged regions (5.3%), and few commission errors were found in damaged regions (3.2%). The final binary maps exhibiting damaged vs. non-damaged areas for both methods are depicted on Figure 10. As expected, due to both the optimized segmentation step and the spatio-temporal descriptor introduced, the object-based approach leads to a smoother change detection map.

#### 4.6. Influence of feature selection on classification accuracy

To assess the relevance of our feature selection method, the segmentation of the bi-temporal image was processed using the eight initial bands (i.e. before- and after-storm images) with no feature selection. The overall classification accuracy decreased from 87.8 to 83.3% when using feature selection.

For the K-means pixel-based approach, the best spectral feature led to an overall classification accuracy of 83.2%, which is better than that using the eight initial bands (78.7%). This confirms, in accordance with our object-based approach (see Section 4.1.1), that the use of all bands is not necessarily the best choice for bitemporal segmentation and classification and that a feature selection process improves the classification results.

##### 4.6.1. Comparison to age class map

The INRA geodatabase, which collects the ages of all pine stands, was compared to the obtained classification. The accuracy assessment is detailed according to age class in Table 5.

Table 5. Confusion matrix according to age class.

Age class	Number of pixels	Omission error (%)		Commission error (%)		Overall accuracy per age class (%)
		Non-damage	Damage	Non-damage	Damage	
5 – 9	115	0	100	40.0	100	60.0
10 – 13	510	0	99.0	59.0	100	41.4
14 – 20	1406	0.76	12.0	11.9	0.76	93.3
21 – 25	424	6.25	0	0	10.1	96.0
26 – 30	694	9.30	0	0	0.61	99.4
31 – 39	1086	26.3	0	0	5.53	95.2
>39	193	11.1	30.3	76.8	1.61	71.5

The percentage of pixels classified as damaged (damage rate) was computed within each age class and the results are shown in Figure 11, which also depicts the behaviour of the overall classification accuracy with respect to each age class. This figure shows that classification accuracy increases significantly with stand age. In fact, tree sensitivity to wind increases with tree height, which depends on tree age (Cucchi et al. 2005). This effect is confirmed by the Formosat-2-derived damage rate, which was higher for older stands and reached 70% for stands over 25 years old. This is a good indicator of the quality of the results obtained.

Table 5 shows that the classification accuracy of stands aged from 14 to 39 years (four intermediate classes) is high and ranges between 93.3 and 99.4%. However, the two youngest classes and the oldest stand class have lower detection rates (60, 41.4, and 71.5%, respectively) resulting from high omission and commission errors (>30%). Confusion occurred between damaged areas and non-damaged older areas, which were originally heterogeneous and sparse. In fact, both areas have similar spectral properties and textural structure. In addition, subtle change areas with minor tree damage (bent trees) were hard to detect in dense young stands. In addition, very small intact or damaged areas cannot be detected due to the limited spatial resolution of Formosat-2 images. Finally, in our method, shadows are not explicitly taken into account in segmentation or in

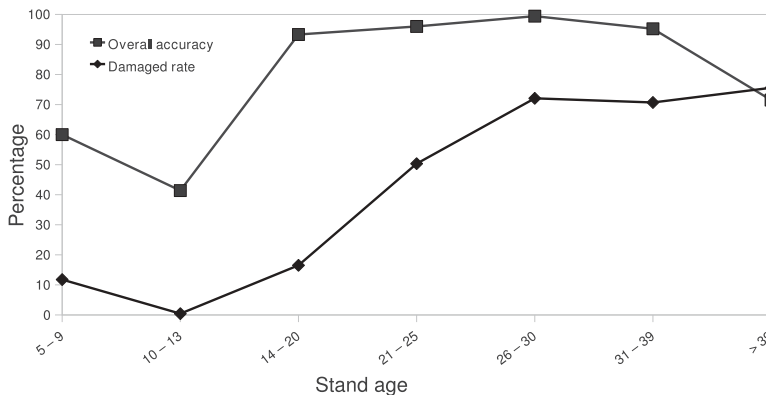


Figure 11. Overall classification accuracy and damage rate as a function of age class.

classification, potentially leading to misclassifications. With only one image dataset, we were unable to estimate the influence of shadows or viewing angle on the outcome of the change detection. These issues should be further developed in future work.

## 5. Conclusion

We have presented in this paper an object-based bitemporal change detection method that is well suited to emergency mapping. It has the appealing property of requiring only a few samples to construct the test frames, leading to a low requirement for supervision compared with more traditional supervised methods. Moreover, our method involves only two user-defined parameters and does not need to meet any statistical assumptions, thanks to the powerful MS clustering algorithm at the core of our change detection scheme.

Our contribution comprises two main novelties with respect to similar works in forestry. First, an automatic feature selection process, applied to both the segmentation and classification steps, is introduced. Its originality lies in the use of test frames (single- or multibands) of adequate forest samples. This innovative feature selection process, inspired by camera calibration procedures, allows a rapid evaluation of hundreds of features and combined features. It is applicable to the optimization of any other segmentation algorithm.

The second original feature of our approach is a relevant spatio-temporal descriptor: the FR, which enables a simple automatic binary threshold (damage vs. non-damage) for the various change clusters obtained by the MS classifier. The FR can be applied to other change detection applications assuming that natural processes, either progressive (urbanization) or disastrous (floods, earthquakes, etc.), tend to fragment the landscape.

Our change detection scheme was applied in forestry, in the context of storm damage mapping. Severe damage was accurately detected, and our method yields a good overall accuracy of 87.8

In future work, the radiometric range,  $h_r$ , should be adapted to each feature in the MS algorithm to cover the spectral distribution variability and therefore take advantage of the combination of multiple features. In addition, our MS-based change detection scheme allows the detection of gradual changes. Appropriate reference data should be collected to validate such applications. In addition, our method will be applied to very high-resolution satellite images, such as those of QuickBird, IKONOS, or Pleiade, to evaluate its performance for subtle change detection (e.g. bent trees) and other applications.

## Acknowledgements

The Orfeo programme facilitated the future use of the VHR Pleiades images. Access to the images was granted by the CNES Kalideos Programme (<http://Kalideos.cnes.fr>). The images were analysed using the OTB toolbox ([www.orfeo-toolbox.org](http://www.orfeo-toolbox.org)). The authors also acknowledge Olivier Hagolle (CNES/Cesbio, Toulouse), and Christophe Moisy (INRA, EPHYSE, Bordeaux) for image preprocessing.

## Funding

The present study was carried out within the Orfeo programme funded by CNES (Centre National d'Etudes Spatiales). The authors also acknowledge INRA for the funding of the orthophotographs within *Crédit tempête 2009*.

## Note

1. Institut National de Recherches Agronomiques (French National Institute of Agricultural research).

## References

- Benz, U. C., P. Hofmann, G. Willhauck, I. Lingenfelder, and M. Heynen. 2004. "Multi-Resolution, Object-Oriented Fuzzy Analysis of Remote Sensing Data for Gis-Ready Information." *ISPRS Journal of Photogrammetry and Remote Sensing* 58 (3–4): 239–258. doi:10.1016/j.isprsjprs.2003.10.002.
- Blaschke, T. 2010. "Object Based Image Analysis for Remote Sensing." *ISPRS Journal of Photogrammetry and Remote Sensing* 65 (1): 2–16. doi:10.1016/j.isprsjprs.2009.06.004.
- Chehata, N., C. Orny, S. Boukir, and D. Guyon. 2011. "Object-Based Forest Change Detection Using High Resolution Satellite Images." In *PIA11, International Archives of Photogrammetry, Remote Sensing and Spatial Information Sciences XXXVIII*, edited by U. Stilla, F. Rottensteiner, H. Mayer, B. Jutzi, and M. Butenuth, Vol. 3/W22, Munich, October 5–7, 49–55.
- Clandillon, S., H. Yesou, and C. Meyer. 2003. "Benefits of SPOT 5 HR and VHR Data for Forest Management and Windfall Damage Mapping." In *IEEE International Geoscience and Remote Sensing Symposium, IGARSS '03*, Vol. 5, Toulouse, 3079–3081. IEEE. doi:10.1109/IGARSS.2003.1294689.
- Comaniciu, D., and P. Meer. 2002. "Mean Shift: A Robust Approach toward Feature Space Analysis." *IEEE Transactions on Pattern Analysis and Machine Intelligence* 24 (5): 603–619. doi:10.1109/34.1000236.
- Conchedda, G., L. Durieux, and P. Mayaux 2008. "An Object-Based Method for Mapping and Change Analysis in Mangrove Ecosystems." *ISPRS Journal of Photogrammetry and Remote Sensing* 63 (5): 578–589. Remote Sensing of the Coastal Ecosystems Special Issue. doi:10.1016/j.isprsjprs.2008.04.002.
- Cucchi, V., C. Meredieu, A. Stokes, F. Coligny, J. Suarez, and B. A. Gardiner. 2005. "Modelling the Windthrow Risk for Simulated Forest Stands of Maritime Pine (*Pinus Pinaster Ait.*)." *Forest Ecology and Management* 213: 184–196. doi:10.1016/j.foreco.2005.03.019.
- Desclée, B., P. Bogaert, and P. Defourny. 2006. "Forest Change Detection by Statistical Object-Based Method." *Remote Sensing of Environment* 102 (1–2): 1–11. doi:10.1016/j.rse.2006.01.013.
- Duda, R. O., P. E. Hart, and D. G. Stork. 2001. *Pattern Classification*. 2nd ed. New York: Wiley-Interscience.
- Franklin, S. E., R. H. Waring, R. W. McCreight, W. B. Cohen, and M. Fiorella. 1995. "Aerial and Satellite Sensor Detection and Classification of Western Spruce Budworm Defoliation in a Subalpine Forest." *Canadian Journal of Remote Sensing* 21: 299–308.
- Fraser, R. H., A. Abuelgasim, and R. Latifovic. 2005. "A Method for Detecting Large-Scale Forest Cover Change Using Coarse Spatial Resolution Imagery." *Remote Sensing of Environment* 95 (4): 414–427. doi:10.1016/j.rse.2004.12.014.
- Fukunaga, K., and L. Hostetler. 1975. "The Estimation of the Gradient of a Density Function, with Applications in Pattern Recognition." *IEEE Transactions on Information Theory* 21: 32–40. doi:10.1109/TIT.1975.1055330.
- Garestier, F., P. Dubois-Fernandez, D. Guyon, and T. Le Toan. 2009. "Forest Biophysical Parameter Estimation Using L- and P-Band Polarimetric SAR Data." *IEEE Transactions on Geoscience and Remote Sensing* 47 (10): 3379–3388. doi:10.1109/TGRS.2009.2022947.
- Guyon, D., I. Champion, C. Meredieu, A. Kruszewski, and T. Labbe. 2005. *Final Report – Work Package 1-1 "Ground Data Base"*, April 2005. Technical Report, INRA/Egyptsar04/IC01 and ESTEC-European Space Agency, Contract 18507/04, 18.
- Guyon, D., G. Courier, and P. Berbigier. 2001. "Sensitivity Analysis of Coniferous Forest Reflectance with Canopy Structure and Undergrowth Characteristics from Satellite Data and Modelling (Case Study: Landes Maritime Pine Forest)." In *8th International Symposium "Physical Measurements and Signatures in Remote Sensing"*, edited by CNES, Aussois, January, 387–392.

- Haralick, R. M., K. Shanmugam, and I. Dinstein. 1973. "Textural Features for Image Classification." *IEEE Transactions on Systems, Man, and Cybernetics* 3: 610–621. doi:10.1109/TSMC.1973.4309314.
- Hayes, D. J., and W. B. Cohen. 2007. "Spatial, Spectral and Temporal Patterns of Tropical Forest Cover Change as Observed with Multiple Scales of Optical Satellite Data." *Remote Sensing of Environment* 106 (1): 1–16. doi:10.1016/j.rse.2006.07.002.
- Huang, C., K. Song, S. Kim, J. R. G. Townshend, P. Davis, J. G. Masek, and S. N. Goward. 2008. "Use of a Dark Object Concept and Support Vector Machines to Automate Forest Cover Change Analysis." *Remote Sensing of Environment* 112 (3): 970–985. doi:10.1016/j.rse.2007.07.023.
- Im, J., and J. R. Jensen. 2005. "A Change Detection Model Based on Neighborhood Correlation Image Analysis and Decision Tree Classification." *Remote Sensing of Environment* 99 (3): 326–340. doi:10.1016/j.rse.2005.09.008.
- Johansen, K., L. A. Arroyo, S. Phinn, C. Witte, R. J. Kauth, and G. S. Thomas. 2010. "Comparison of Geo-Object Based and Pixel-Based Change Detection of Riparian Environments Using High Spatial Resolution Multi-Spectral Imagery." *Photogrammetric Engineering and Remote Sensing* 76 (2): 123–136. doi:10.14358/PERS.76.2.123.
- Johansen, K., N. C. Coops, S. E. Gergel, and Y. Stange. 2007. "Application of High Spatial Resolution Satellite Imagery for Riparian and Forest Ecosystem Classification." *Remote Sensing of Environment* 110 (1): 29–44. doi:10.1016/j.rse.2007.02.014.
- Jonikavičius, D., and G. Mozgeris. 2013. "Rapid Assessment of Wind Storm-Caused Forest Damage Using Satellite Images and Stand-Wise Forest Inventory Data." *iforest* 6: 150–155. doi:10.3832/ifor0715-006.
- Kayitakire, F., C. Hamel, and P. Defourny. 2006. "Retrieving Forest Structure Variables Based on Image Texture Analysis and IKONOS-2 Imagery." *Remote Sensing of Environment* 102: 390–401. doi:10.1016/j.rse.2006.02.022.
- Kennedy, R. E., P. A. Townsend, J. E. Gross, W. B. Cohen, P. Bolstad, Y. Q. Wang, and P. Adams. 2009. "Remote Sensing Change Detection Tools for Natural Resource Managers: Understanding Concepts and Tradeoffs in the Design of Landscape Monitoring Projects." *Remote Sensing of Environment* 113 (7): 1382–1396. doi:10.1016/j.rse.2008.07.018.
- Kim, M., M. Madden, and T. Warner. 2008. "Estimation of Optimal Image Object Size for the Segmentation of Forest Stands with Multispectral IKONOS Imagery." In *Object-Based Image Analysis*, edited by T. Blaschke, S. Lang, and G. J. Hay, 291–307. Lecture Notes in Geoinformation and Cartography. Berlin: Springer.
- King, D. J., I. Olthof, P. K. E. Pellikka, E. D. Seed, and C. Butson. 2005. "Modelling and Mapping Damage to Forests from an Ice Storm Using Remote Sensing and Environmental Data." *Natural Hazards* 35: 321–342. doi:10.1007/s11069-004-1795-4.
- Lamonaca, A., P. Corona, and A. Barbati. 2008. "Exploring Forest Structural Complexity by Multi-Scale Segmentation of VHR Imagery." *Remote Sensing of Environment* 112 (6): 2839–2849. doi:10.1016/j.rse.2008.01.017.
- Liu, D., K. Song, J. R. G. Townshend, and P. Gong. 2008. "Using Local Transition Probability Models in Markov Random Fields for Forest Change Detection." *Remote Sensing of Environment* 112 (5): 2222–2231. Earth Observations for Terrestrial Biodiversity and Ecosystems Special Issue. doi:10.1016/j.rse.2007.10.002.
- Mäkelä, H., and A. Pekkarinen. 2001. "Estimation of Timber Volume at the Sample Plot Level by Means of Image Segmentation and Landsat TM Imagery." *Remote Sensing of Environment* 77: 66–75. doi:10.1016/S0034-4257(01)00194-8.
- Mallinis, G., N. Koutsias, M. Tsakiri-Strati, and M. Karteris. 2008. "Object-Based Classification Using Quickbird Imagery for Delineating Forest Vegetation Polygons in a Mediterranean Test Site." *ISPRS Journal of Photogrammetry and Remote Sensing* 63 (2): 237–250. doi:10.1016/j.isprsjprs.2007.08.007.
- McRoberts, R. E., and B. F. Walters. 2012. "Statistical Inference for Remote Sensing-Based Estimates of Net Deforestation." *Remote Sensing of Environment* 124: 394–401. doi:10.1016/j.rse.2012.05.011.
- Meyer, C., P. Geldreich, and H. Yesou. 2001. "Apports des Données Simulées SPOT5 Pour l'Évaluation Des Dégâts De Tempête Dans La Forêt. Cas De La Forêt De Haguenau (Alsace, France)." In *Bulletin de la Société Française de Photogrammétrie et de Télédétection*, No. 164–165 (2001-4/2002-1): 162–173.

- Olthof, I., D. J. King, and R. A. Lautenschlager. 2004. "Mapping Deciduous Forest Ice Storm Damage Using Landsat and Environmental Data." *Remote Sensing of Environment* 89: 484–496. doi:10.1016/j.rse.2003.11.010.
- Orny, C., N. Chehata, S. Boukir, and D. Guyon. 2010. *Characterization of Maritime Pine Forest Structure Changes with VHR Satellite Imagery: Application to the 24th January 2009 Windfall Damages Cartography*. Technical Report. Toulouse: CNES.
- Otsu, N. 1979. "A Threshold Selection Method from Gray-Level Histograms." *IEEE Transactions on Systems, Man and Cybernetics* 9: 62–66. doi:10.1109/TSMC.1979.4310076.
- Ozdarici, O. A., and Z. Akyurek. 2012. "A Segment-Based Approach to Classify Agricultural Lands by Using Multi-Temporal Optical and Microwave Data." *International Journal of Remote Sensing* 33 (22): 7184–7204. doi:10.1080/01431161.2012.700423.
- Pasher, J., and D. J. King. 2009. "Mapping Dead Wood Distribution in a Temperate Hardwood Forest Using High Resolution Airborne Imagery." *Forest Ecology and Management* 258: 1536–1548. doi:10.1016/j.foreco.2009.07.009.
- Ruiz, L. A., A. Fdez-sarria, and J. A. Recio. 2004. "Texture Feature Extraction for Classification of Remote Sensing Data Using Wavelet Decomposition: A Comparative Study." *International Archives of Photogrammetry and Remote Sensing XXXV*: 1682–1750.
- Schwarz, M., C. Steinmeier, and L. Waser. 2001. "Detection of Storm Losses in Alpine Forest Areas by Different Methodic Approaches Using High Resolution Satellite Data." In *Proceedings of the 21st EARSeL Symposium: Observing Our Environment from Space: New Solutions for a New Millenium*, 251–257.
- St-Louis, V., A. M. Pidgeon, V. C. Radeloff, T. J. Hawbaker, and M. K. Clayton. 2006. "Highresolution Image Texture as a Predictor of Bird Species Richness." *Remote Sensing of Environment* 105: 299–312. doi:10.1016/j.rse.2006.07.003.
- Trias-Sanz, R., G. Stamon, and J. Louchet. 2008. "Using Colour, Texture, and Hierarchical Segmentation for High-Resolution Remote Sensing." *ISPRS Journal of Photogrammetry and Remote Sensing* 63: 156–168. doi:10.1016/j.isprsjprs.2007.08.005.
- Tuominen, S., and A. Pekkarinen. 2005. "Performance of Different Spectral and Textural Aerial Photograph Features in Multi-Source Forest Inventory." *Remote Sensing of Environment* 94: 256–268. doi:10.1016/j.rse.2004.10.001.
- Vibrans, A. C., R. E. McRoberts, P. Moser, and A. L. Nicoletti. 2013. "Using Satellite Image-Based Maps and Ground Inventory Data to Estimate the Area of the Remaining Atlantic Forest in the Brazilian State of Santa Catarina." *Remote Sensing of Environment* 130: 87–95. doi:10.1016/j.rse.2012.10.023.
- Wang, W., J. J. Qu, X. Hao, Y. Liu, and J. A. Stanturf. 2010. "Post-Hurricane Forest Damage Assessment Using Satellite Remote Sensing." *Agricultural and Forest Meteorology* 150: 122–132. doi:10.1016/j.agrformet.2009.09.009.
- Wang, Y., Y. S. Soh, and H. Shultz. 2006. "Individual Tree Crown Segmentation in Aerial Forestry Images by Mean Shift Clustering and Graph-Based Cluster Merging." *International Journal of Computer Science and Network Security* 6 (11): 40–45.
- Wang, F., and Y. J. Xu. 2010. "Comparison of Remote Sensing Change Detection Techniques for Assessing Hurricane Damage to Forests." *Environmental Monitoring and Assessment* 162: 311–326. doi:10.1007/s10661-009-0798-8.
- Wulder, M. A., J. C. White, N. C. Coops, and C. R. Butson. 2008. "Multi-Temporal Analysis of High Spatial Resolution Imagery for Disturbance Monitoring." *Remote Sensing of Environment* 112 (6): 2729–2740. doi:10.1016/j.rse.2008.01.010.

Copyright of International Journal of Remote Sensing is the property of Taylor & Francis Ltd and its content may not be copied or emailed to multiple sites or posted to a listserv without the copyright holder's express written permission. However, users may print, download, or email articles for individual use.